

On-chip quantum NOON state sensing for temperature and humidity

Weihong Luo(罗伟宏), Chao Wu(吴超), Yuxing Du(杜昱星), Chang Zhao(赵畅), Miaomiao Yu(余苗苗), Pingyu Zhu(朱枰谕), Kaikai Zhang(张凯凯), and Ping Xu(徐平)

Citation: Chin. Phys. B, 2024, 33 (**10**): 100305. DOI: 10.1088/1674-1056/ad72e2
Journal homepage: http://cpb.iphy.ac.cn; http://iopscience.iop.org/cpb

What follows is a list of articles you may be interested in

Enhanced measurement precision with continuous interrogation during dynamical decoupling

Jun Zhang(张军), Peng Du(杜鹏), Lei Jing(敬雷), Peng Xu(徐鹏), Li You(尤力), and Wenxian Zhang(张文献)
Chin. Phys. B, 2024, 33 (**3**): 030301. DOI: 10.1088/1674-1056/ad1985

Long-range interacting Stark many-body probes with super-Heisenberg precision

Rozhin Yousefjani, Xingjian He(何行健), and Abolfazl Bayat
Chin. Phys. B, 2023, 32 (**10**): 100313. DOI: 10.1088/1674-1056/acf302

Orientation determination of nitrogen-vacancy center in diamond using a static magnetic field

Yangpeng Wang(王杨鹏), Rujian Zhang(章如健), Yan Yang(杨燕), Qin Wu(吴琴), Zhifei Yu(于志飞), and Bing Chen(陈冰)
Chin. Phys. B, 2023, 32 (**7**): 070301. DOI: 10.1088/1674-1056/acc0f7

Fringe removal algorithms for atomic absorption images: A survey

Gaoyi Lei(雷高益), Chencheng Tang(唐陈成), and Yueyang Zhai(翟跃阳)
Chin. Phys. B, 2022, 31 (**5**): 050313. DOI: 10.1088/1674-1056/ac3758

Optical scheme to demonstrate state-independent quantum contextuality

Ya-Ping He(何亚平), Deng-Ke Qu(曲登科), Lei Xiao(肖磊), Kun-Kun Wang(王坤坤), and Xiang Zhan(詹翔)
Chin. Phys. B, 2022, 31 (**3**): 030305. DOI: 10.1088/1674-1056/ac229f

---

SPECIAL TOPIC — Quantum computing and quantum sensing

On-chip quantum NOON state sensing for temperature and humidity

Weihong Luo(罗伟宏)[†], Chao Wu(吴超)[†], Yuxing Du(杜昱星)[†], Chang Zhao(赵畅), Miaomiao Yu(余苗苗), Pingyu Zhu(朱枰谕), Kaikai Zhang(张凯凯), and Ping Xu(徐平)[‡]

Institute for Quantum Information & State Key Laboratory of High Performance Computing, College of Computer Science and Technology, National University of Defense Technology, Changsha 410073, *China*

(Received Received 17 July 2024; revised manuscript received 23 August 2024; accepted manuscript online 23 August 2024)

A maximal photon number entangled state, namely NOON state, can be adopted for sensing with a quantum enhanced precision. In this work, we designed silicon quantum photonic chips containing two types of Mach–Zehnder interferometers wherein the two-photon NOON state, sensing element for temperature or humidity, is generated. Compared with classical light or single photon case, two-photon NOON state sensing shows a solid enhancement in the sensing resolution and precision. As the first demonstration of on-chip quantum photonic sensing, it reveals the advantages of photonic chips for high integration density, small-size, stability for multiple-parameter sensing serviceability. A higher sensing precision is expected to beat the standard quantum limit with a higher photon number NOON state.

Keywords: quantum sensing, NOON state, photonic chip

PACS: 03.67.–a, 42.50.Dv, 42.82.–m, 42.65.–k **DOI:** 10.1088/1674-1056/ad72e2

1. Introduction

The measurement of temperature and humidity has been widely used in various fields, ranging from biological monitoring and chemical analysis to environmental observation and industrial manufacturing.[1–5] In recent years, optical sensors are emerging as alternative approaches to resistance thermometers and hygrometers, owing to their advantages of high sensitivity, fast response, and immunity to electromagnetic interference and mechanical shocks. The proposed fiber-based sensing devices are mainly based on macroscale fiber Bragg grating,[6] fiber Fabry–Pérot (FP) cavities,[7] photonic crystal fiber,[8,9] etc. Thanks to the advantages of low-cost, compact size, and complementary metal–oxide–semiconductor compatibility, integrated silicon waveguides based sensors have attracted much interest, thus prospering various sensing structures including micro-ring resonators,[10,11] Mach–Zehnder interferometer (MZI),[12,13] FP cavities,[14] and waveguide Bragg gratings.[15]

The sensitivity of sensors is a crucial indicator for performance evaluation. In the case of the silicon-based sensors, the temperature sensitivity is typically constrained to around 80 pm/°C due to the thermo-optic coefficient (TOC) of silicon.[16–18] Consequently, substantial efforts have focused on enhancing this sensitivity through techniques such as waveguide group index engineering,[19] leveraging the Vernier effect with cascaded ring resonators,[20] utilizing cascaded silicon photonic crystal (PhC) nanobeam cavities,[21] incorporating waveguides with large negative TOC in the cladding,[16] and exploring polymer hybrid waveguides.[12]

Currently, photonic quantum sensing is gaining interest as attractive avenues to enhancing sensitivity and achieving super-precision measurement surpassing standard quantum limit (SQL). In particular, multi-photon maximally entangled states,[22] commonly known as NOON states, have garnered substantial attention in this field. The NOON state is commonly used in quantum optics and quantum information science. Its name comes from its representation, its standard form is

$$\Psi_{\mathrm{NOON}} = \frac{1}{\sqrt{2}}(|N,0\rangle_{a,b} + |0,N\rangle_{a,b}), \tag{1}$$

where N represents the number of photons either in mode a or b, 0 indicates the absence of photons in this mode. A universal scheme for preparing three- and four-photon path-entangled NOON states on a photonic chip has been proposed.[23] According to the central limit theorem from classical probability theory, as the number of entangled particles N increases during repetitive experiments, the estimated standard deviation reduces by a factor proportional to $\sqrt{N}$. Up to now, it has been reported that NOON states with $N = 2$ photons can beat the SQL in phase sensing experiments,[26] and a Sagnac bulk optics with 4-photon has exhibited quantum enhanced resolution and precision.[27] However, the on-chip quantum photonic sensing with NOON states has not been designed, further the performance of such integrated version for temperature and humidity sensing which moves a further step towards practical use is highly designed.

Here, we designed and manufactured silicon quantum photonic chips consisting of Mach–Zehnder interferometers (MZI) wherein quantum light sources,[28] the sensing arm and the control arm are integrated, and experimentally realized

[†]These authors contributed equally to this work.

[‡]Corresponding author. E-mail: pingxu520@nju.edu.cn

© 2024 Chinese Physical Society and IOP Publishing Ltd

the sensitivity enhancement of temperature and humidity. For temperature sensing, an asymmetric Mach–Zehnder interferometer (AMZI) is designed after the two-photon NOON state is generated in the two arms of MZI. For humidity sensing, a local opening cladding layer is required and the moisture-sensitive materials are coated on the silicon waveguide. Compared to the classical light or single photon methods, two-photon NOON state sensing shows a solid enhancement in the sensing resolution and precision. Furthermore, our design can be easily extended to more photons and other integrated platforms.

2. Experimental setup

As one of the prevalent interferometric designs, MZI plays a pivotal role in various optical sensing and phase measurement applications.[29] Figure 1(a) illustrates a standard MZI setup. Assuming symmetrical beam splitters and interference arms of equal length, the evolution of a single-photon state through the MZI and its resulting output state can be represented as

$$\frac{1}{2}[(1-\mathrm{e}^{\mathrm{i}\varphi})e^{\dagger}+\mathrm{i}(1+\mathrm{e}^{\mathrm{i}\varphi})f^{\dagger}]\,|0\rangle\,. \tag{2}$$

When single-photon detection is performed at the output ports e and f, the probabilities of detection are given by

$$P_e=|\frac{1}{2}(1-\mathrm{e}^{\mathrm{i}\varphi})|^2=\frac{1}{2}(1-\cos\varphi), \tag{3}$$

$$P_f=|\frac{\mathrm{i}}{2}(1+\mathrm{e}^{\mathrm{i}\varphi})|^2=\frac{1}{2}(1+\cos\varphi). \tag{4}$$

We have thus far discussed the evolution of single photon states in MZI. In our experiment, obtaining a probability $P=(1-\cos\varphi)/2$ allows us to estimate φ. Here φ is the relative phase between two arms of MZI and may result from the variation of temperature or humidity, hence the MZI can be adopted for photonic sensing. Remarkably, by generating a maximal photon number entangled state within the interferometer, SQL can be surpassed and even higher precision in sensor measurements can be attained.

Considering the scenario where one photon is introduced at each of the two inputs of the MZI, two indistinguish noiseable photons are injected into two sides of the interferometer (ports a and b), respectively, in this case of a two-photon MZI. The resultant output state can be described as follows:

$$\frac{1}{4}[\mathrm{i}(\mathrm{e}^{\mathrm{i}2\varphi}-1)e^{\dagger}e^{\dagger}-(2\mathrm{e}^{\mathrm{i}2\varphi}+2)e^{\dagger}f^{\dagger} +\mathrm{i}(1-\mathrm{e}^{\mathrm{i}2\varphi})f^{\dagger}f^{\dagger}]\,|00\rangle\,. \tag{5}$$

From this evolution, we deduce that the probability of detecting a photon at both outputs e and f is $P_{ef}=(1+\cos 2\varphi)/2$. Notably, compared to the single-photon MZI, the two-photon version offers twice the sensitivity in sensing φ.

Figure 1(b) depicts the schematic diagram of the chip structure we have designed, which is a modified version of Fig. 1(a). It principally includes the beam splitting of the pump light, the preparation of a path-entangled two-photon state, a sensing unit, and the interference measurement of the two-photon state. The pump light is fed into the chip through the coupling of the optical fiber array and the grating coupler located on the chip, and then bifurcates into two paths via the MZI. The phase of the interferometer is adjusted by a thermo-optic phase shifter integrated on one arm of the MZI's waveguide, ensuring that the pump optical power is identical in both arms. Subsequently, the two pumped light beams enter two bent and coiled single-mode waveguides, each with a length of 1 cm, where a spontaneous four-wave mixing (SFWM) effect occurs and the signal and idler photon pair is generated in either arm indistinguishably, resulting in a path-entangled two-photon state of $(1/\sqrt{2})(|20\rangle+|02\rangle)$, so we prepared a NOON state with $N=2$.

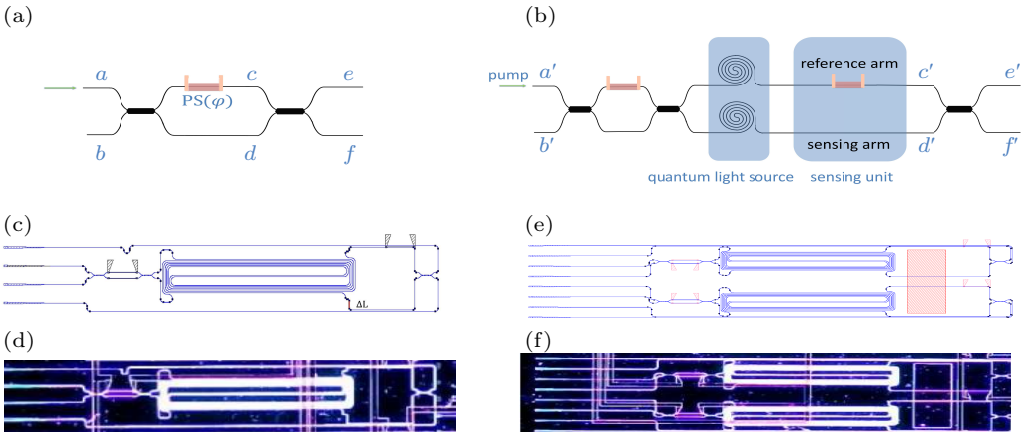


Fig. 1. (a) Typical Mach–Zehnder interferometer structure, photons are introduced via port a or simultaneously through ports a and b, and subsequently detected at ports e and f. (b) Sensor chip schematic, featuring a MZI for the division of the pumping light beam, a quantum light source, and a sensing unit. (c) Design diagram of the temperature sensor chip, $\Delta L=87.964$ μm. (d) Microscope illustration of temperature sensor chip. (e) Design diagram of the humidity sensor chip, The red areas are the overburden that has been etched away. (f) Microscope illustration of humidity sensor chip.

The sensing unit comprises a reference arm that regulates the initial phase difference between the two arms. The sensing arm is tasked with detecting the phase change induced by the physical quantity under measurement. As the two-photon entangled state traverses the sensing unit, it evolves into

$$\Psi_{c'd'} = \frac{1}{\sqrt{2}}(|20\rangle + \mathrm{e}^{\mathrm{i}2\Delta\varphi}|02\rangle), \tag{6}$$

where $\Delta\varphi$ is modulated by the physical quantity and the thermo-optic phase shifter for a single photon. Here $2\Delta\varphi$ indicates that the signal and idler photons sense the phase twice. After passing through a 50:50 beam splitter interferometer, the two-photon entangled state transforms into

$$\Psi_{e'f'} = \frac{1}{\sqrt{2}}(|20\rangle - |02\rangle)\sin\Delta\varphi + |11\rangle\cos\Delta\varphi. \tag{7}$$

By selecting a base vector such as $|11\rangle$, the interference curve of two-photon coincidence counting varying with phase difference can be obtained as

$$P_{e'f'} = \frac{(1+\cos 2\Delta\varphi)}{2}, \tag{8}$$

which exhibits a twice sensing resolution of phase compared to the single photon or classical case.

We employ Fisher information to assess the feasibility of surpassing SQL.[30] In two-photon NOON state sensing, when the initial phase difference is φ_0, the Fisher information per photon is

$$F_\varphi = \frac{2V^2\sin^2 2\varphi_0}{1 - V^2\cos^2 2\varphi_0}. \tag{9}$$

The F_φ depends on the interference fringe visibility V and the initial phase difference φ_0, SQL corresponds to a Fisher information of one per photon. When $V = 70.7\%$, the peak value of the Fisher information attains SQL threshold, indicating that to surpass this threshold, an experimental interference fringe visibility V must exceed it.

The pump light used in the experiment is 1549.32 nm continuous light, while the entangled photon pairs are 1546.02 nm and 1552.52 nm, respectively. The silicon waveguide's cross-section dimensions are 500 nm wide and 220 nm tall, with a 3 μm thick silica covering and buried layer. The 50:50 beam splitter measures 140 μm × 40.5μm, and the length of thermal phase shifter is 180 μm. The phase shifter of the MZI is achieved by adjusting the power of a DC power supply, thereby modifying the phase difference between the interferometer's dual arms. The power consumption for a π phase shift is 25 mW, which ensures an equal distribution of optical pump power across the two output ports of the interferometer. The silicon waveguide of the spontaneous four-wave mixing source has a length of 1 cm, and the resultant photon pair exhibits a full width at half maximum (FWHM) of 54 nm.

Figure 1(c) illustrates the schematic design of the temperature sensor chip, whereas figure 1(d) presents the microscopic image of the chip. The length discrepancy ΔL between the two arms of the sensing unit is established at 87.964 μm. Consequently, the phase difference $\Delta\varphi$ between the two arms corresponds to the variation in the overall temperature T of the sensing unit:

$$\Delta\varphi = \frac{2\pi}{\lambda} \times \mathrm{RIU} \times \Delta L \times T, \tag{10}$$

where λ is the wavelength, and $\mathrm{RIU} = \mathrm{d}n/\mathrm{d}T$ represents the alteration in the effective refractive index n of the silicon waveguide per unit temperature change. For our silicon waveguide configuration, the RIU is approximately 1.87×10^{-4} °C^{-1}. So in classical case, the temperature changes by 47 °C, and the relative phase $\Delta\varphi$ between the states on the two arms of the interferometer changes by π, then in two-photon NOON state, the temperature changes by only 23.5 °C, the relative phase $\Delta\varphi$ between the states on the two arms of the interferometer changes by π.

The structural configuration of the optical quantum chip for humidity quantum sensing closely resembles that of temperature sensing, comprising three primary components: the classical laser processing unit, the nonlinear processing unit, and the sensing unit. Specifically, the classical laser and nonlinear processing units are identical to those utilized in the temperature sensor chip design. However, the sensing unit of the humidity sensor chip diverges from that of the temperature sensor chip. The schematic representation of the humidity sensor chip is depicted in Fig. 1(e), and figure 1(f) illustrates the chip as observed under a microscope. Within the sensing unit, both arms are of equal length, and the silica covering layer of the silicon waveguide on the sensing arm is etched and exposed to the ambient air. The etched length L is 300 μm, to enhance the sensitivity of the sensing arm to humidity, we applied agarose gel to the etched area. Then the phase difference $\Delta\varphi$ of the two arms is satisfied with the change of the humidity h of the sensing unit:

$$\Delta\varphi = \frac{2\pi}{\lambda} \times \mathrm{RIUhf} \times L \times h, \tag{11}$$

where λ is the wavelength, and $\mathrm{RIUhf} = \mathrm{d}n/\mathrm{d}h$ represents the alteration in the effective refractive index n of the windowed part of the waveguide due to a unit change in humidity. In our silicon waveguide design, the refractive index of the agarose gel changes due to the change of humidity, which affects the effective refractive index of the waveguide in the etched area. We calculated through simulation that the RIUhf is approximately 4.41×10^{-5}/%RH. So in classical case, the humidity changes by 58.6%RH, and the relative phase $\Delta\varphi$ between the states on the two arms of the interferometer changes by π, then in two-photon NOON state, the humidity changes by only

29.3%RH, the relative phase $\Delta\varphi$ between the states on the two arms of the interferometer changes by π.

We constructed the light path according to the experimental design. The main components of the optical path include 10 mW continuous laser with the wavelength of 1549.32 nm, ThorLabs PM100USB power meters, constant temperature and humidity box, superconducting nanowire single photon detectors (SNSPDs) and a silicon based optical quantum sensor chip, as depicted in Fig. 2. The optical quantum chip has been coupled with the optical array through optical packaging, and the corresponding optical fiber port can be directly connected during the experiment, without re-coupling.

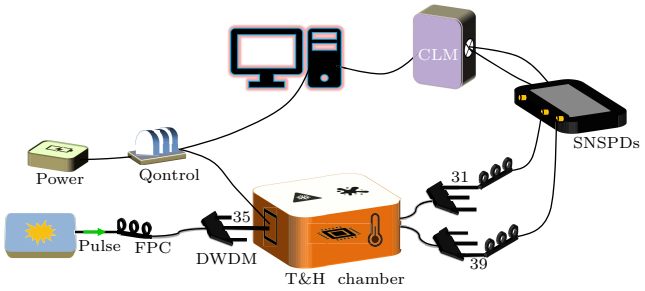


Fig. 2. Schematic diagram of experimental light path construction.

Additionally, the chip is also electrically packaged and connected to the electronic control equipment by wiring according to the layout. The packaged optical quantum chip is placed in the constant temperature and humidity box, the optical fiber array is pulled out of the opening of the constant temperature and humidity box, and the probe of the temperature and the humidity measuring instrument is placed near the optical quantum chip through the opening.

3. Results

The constant temperature and humidity box was initially set to a specific temperature value, with a temperature increase step of 2 °C. The thermo-optic phase shifter on the MZI arm was adjusted for both classical and quantum sensing to ensure they operated within the same temperature range. Subsequently, the relationship curve between power value and temperature measured under classical sensing and the relationship curve between coincidence count and temperature under quantum sensing are drawn. Perform triangular curve fitting on the experimental result data, as shown in Fig. 3(a). In classical case, when the temperature changes by 41.9 °C, the relative phase $\Delta\varphi$ changes by π. With two-photon NOON state, when the temperature changes by 21 °C, the relative phase $\Delta\varphi$ changes by π. As a result, within a reasonable error range, the resolution of temperature quantum sensing is about twice that of classical case, which verifies our theory. Then we calculate the experimentally measured $\mathrm{RIU}' \approx 2.09\times10^{-4}\ ^\circ\mathrm{C}^{-1}$. Compared with the theoretical value of $1.87\times10^{-4}\ ^\circ\mathrm{C}^{-1}$, there is an error of about 11.8%. The observed error may arise from multiple factors, for instance, the thermal conductivity limitations of the chip can hinder the sensor's ability to accurately detect the ambient temperature. Furthermore, there may be inherent inaccuracies in the ambient temperature readings obtained from the thermometer utilized in our experiment.

The experimental data for both classical and quantum sensing were normalized, and the section of the trigonometric function exhibiting near-linear change was extracted. After fitting, in classical sensing, the relationship between the power meter reading p_t and temperature t is expressed as $p_t = 0.04t - 0.7$, where $p_t \in [0,1]$ indicates the range of power meter readings from minimum to maximum. In quantum sensing, the relationship between the coincidence count value cc_t and temperature t is expressed as $cc_t = 0.08t - 2.3$, where $cc_t \in [0,1]$ indicates the range of coincidence count value from minimum to maximum. Figure 3(b) shows a comparison between classical sensing and quantum sensing. The differential slopes of the curves indicate that quantum temperature sensing achieves a twofold enhancement in phase sensitivity relative to its classical counterpart.

In quantum temperature sensing, the interference fringe visibility V is about 90.4%. As shown in Eq. (9), when we take $\varphi_0 = \pi/4$, $F_\varphi \approx 1.63 > 1$, indicating that the SQL has been beaten in quantum temperature sensing.

Based on a thorough analysis of humidity sensing principles, the humidity sensing employed in this study utilizes the physical adsorption between agarose material and ambient water molecules to achieve environmental water absorption and humidity measurement. After a comparative literature review, we opted to prepare agarose gel using a 0.25% agarose solution. The constant temperature and humidity box was set to an initial humidity value, with a humidity increase step of 5%RH. For classical sensing and quantum sensing, the working interval was adjusted respectively to obtain the measured power value and the coincidence count value. Subsequently, the relationship curve between power value and humidity measured under classical sensing and the relationship curve between coincidence count and humidity under quantum sensing are drawn. Perform triangular curve fitting on the experimental result data, as shown in Fig. 3(c). In classical case, when the humidity changes by 60.1%RH, the relative phase $\Delta\varphi$ changes by π. With two-photon NOON state, when the humidity changes by 31.4%RH, the relative phase $\Delta\varphi$ changes by π. As a result, within a reasonable error range, the resolution of humidity quantum sensing is about twice that of classical case, which verifies our theory. Then we calculate the experimentally measured $\mathrm{RIUhf}' \approx 4.11\times10^{-5}/\%\mathrm{RH}$. Compared with the theoretical value of $4.41\times10^{-5}/\%\mathrm{RH}$, there is an error of about 6.7%. The observed error may arise from multiple factors, for instance, inaccuracies could be present in the concentration of the agarose solution. Additionally, the hygrometer employed for humidity measurement during the

experiment may also exhibit certain discrepancies. In general, these inaccuracies fall within an acceptable range.

The experimental data for both classical and quantum sensing were normalized, and the section of the trigonometric function exhibiting near-linear change was selected. After fitting, in classical sensing, the relationship between the power meter reading p_h and humidity h is expressed as $p_h = 0.02h - 0.38$, where $p_h \in [0, 1]$ indicates the range of power meter readings from minimum to maximum. In quantum sensing, the relationship between the coincidence count value cc_h and humidity h is expressed as $cc_h = 0.04h - 2.2$, where $cc_t \in [0, 1]$ indicates the range of coincidence count value from minimum to maximum. Figure 3(d) shows a comparison between classical sensing and quantum sensing. The differential slopes of the curves indicate that quantum humidity sensing achieves a twofold enhancement in phase sensitivity compared to its classical counterpart.

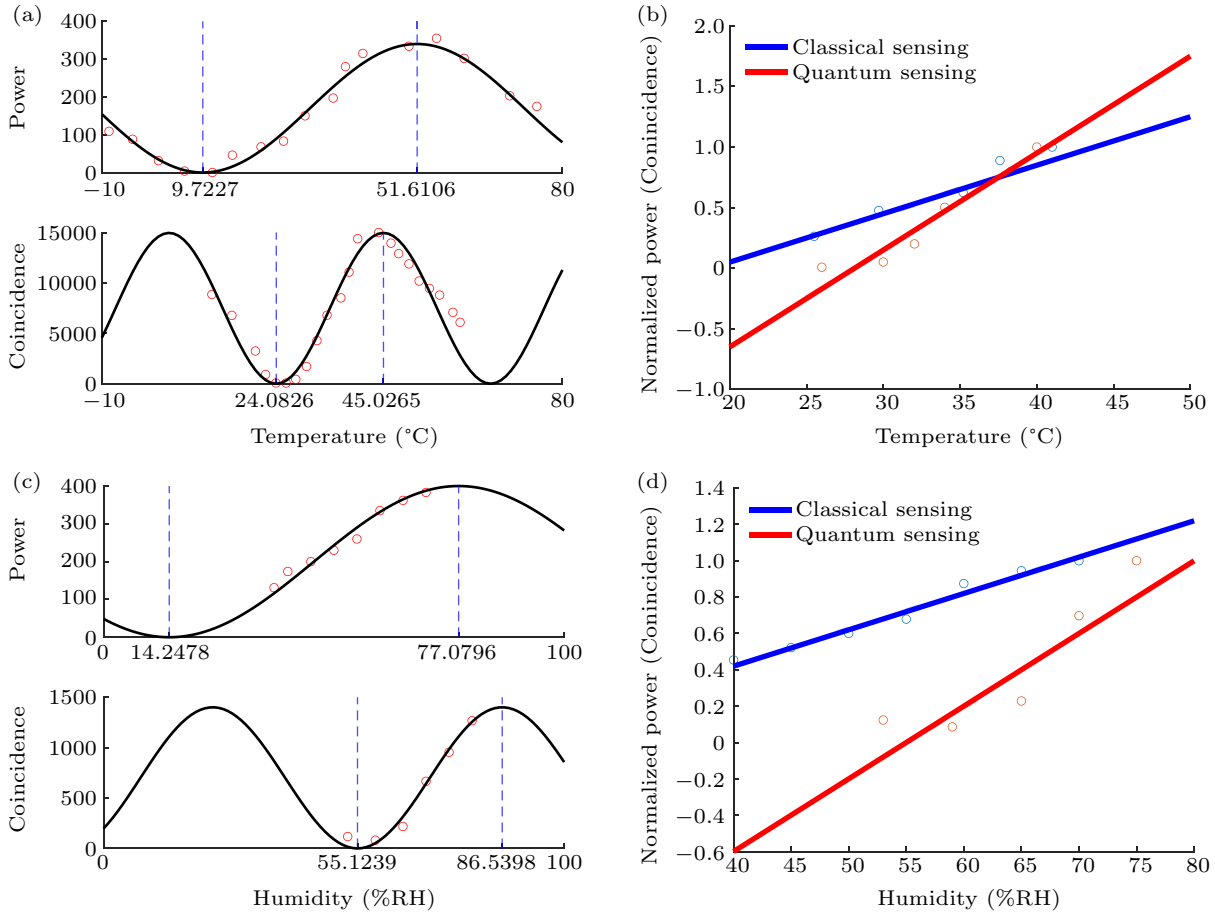


Fig. 3. (a) Experimental results of temperature sensor. (b) Temperature sensing trigonometric function of the linear variation of the region of the fitting curve. (c) Experimental results of humidity sensor. (d) Humidity sensing trigonometric function of the linear variation of the region of the fitting curve.

In quantum humidity sensing, the interference fringe visibility V is about 94%. As shown in Eq. (9), when we take $\varphi_0 = \pi/4$, $F_\varphi \approx 1.77 > 1$, indicating that the SQL has been beaten in quantum humidity sensing.

4. Conclusion

In summary, we have designed a two-photon NOON state Mach–Zehnder interferometer on a silicon chip for temperature and humidity sensing. Our findings demonstrate that both temperature sensing and humidity sensing exhibit a twofold increase in phase sensitivity compared to their classical counterparts. Moving forward, we intend to explore the use of a multi-photon NOON state Mach–Zehnder interferometer for multi-parameter sensing, aiming to achieve an N-fold increase in phase sensitivity. Additionally, the design of AMZI with varying arm lengths can cater to different sensing sensitivity requirements. For instance, a structure with two and three arm length differences offers two and three times the phase sensitivity, respectively, compared to a structure with one arm length difference. Interferometer sensing with different arm lengths has the potential to further enhance the sensing sensitivity.

Acknowledgments

Project supported by the National Key R&D Program of China (Grant No. 2022YFF0712800) and Innova-

tion Program for Quantum Science and Technology (Grant No. 2021ZD0301500).

References

[1] Chao C Y and Guo L J 2003 *Appl. Phys. Lett.* **83** 1527
[2] Xu Q, Almeida V R, Panepucci R R and Lipson M 2004 *Opt. Lett.* **29** 1626
[3] Xu D X, Densmore A, Delage A, Waldron P, McKinnon R, Janz S, Lapointe J, Lopinski G, Mischki T, Post E, Cheben P and Schmid J H 2018 *Opt. Express* **16** 15137
[4] Armani A M, Kulkarni R P, Fraser S E, Flagan R C and Vahala K J 2007 *Science* **317** 783
[5] Chen C, Hou X and Si J H 2017 *Opt. Express* **25** 31294
[6] Zhang B W and Kahrizi M 2007 *IEEE Sens. J.* **7** 586
[7] Lee C E and Taylor H F 1991 *J. Lightwave Technol.* **9** 129
[8] Yu Y Q, Li X L, Hong X M, Deng Y L, Song K Y, Geng Y F, Wei H F and Tong W J 2010 *Opt. Express* **18** 15383
[9] Qian W W, Zhao C L, He S L, Dong X Y, Zhang S Q, Zhang Z X, Jin S Z, Guo J Tao and Wei H F 2011 *Opt. Lett.* **36** 1548
[10] XU H T, Hafezi M, Fan J, Taylor J M, Strouse G F and Ahmed Z 2014 *Opt. Express* **22** 3098
[11] Kim G D, Lee H S, Park C H, Lee S S, Lim B T, Bae H K and Lee W G 2010 *Opt. Express* **18** 22215
[12] Guan X W, Wang X Y and Frandsen L H 2016 *Opt. Express* **24** 16349
[13] Irace A and Breglio G 2003 *Opt. Express* **11** 2807
[14] Pruessner M W, Stievater T H, Ferraro M S and Rabinovich W S 2007 *Opt. Express* **15** 7557
[15] Klimov N N, Mittal S, Berger M and Ahmed Z 2015 *Opt. Lett.* **40** 3934
[16] Teng J, Dumon P, Bogaerts W, Zhang H B, Jian X G, Han X Y, Zhao M S, Morthier G and Baets R 2009 *Opt. Lett.* **17** 14627
[17] Zhou L j, Okamoto K and Yoo S 2009 *IEEE Photon. Technol. Lett.* **21** 1175
[18] Guha B, Cardenas J and Lipson M 2013 *Opt. Lett.* **21** 26557
[19] Zhang Y, Zou J and He J J 2018 *Opt. Express* **26** 26057
[20] Kim H T and Yu M 2016 *Opt. Express* **24** 9501
[21] Zhang Y G, Liu P H, Zhang S L, Liu W X, Chen J Y and Shi Y C 2016 *Opt. Express* **24** 23037
[22] Boto A N, Kok P, Abrams D S, Braunstein S L, Williams C P and Dowling J P 2000 *Phys. Rev. Lett.* **85** 2733
[23] Yu X Y, Zhu P Y, Wang Y, Yu M M, Xue S C, Wu C, Zheng Q L, Liu Y W, Wu J J and Xu P 2022 *Chin. Phys. B* **31** 64203
[24] Lee C, Dieleman F, Lee J Y, Rockstuhl C, Maier S A and Tame M 2016 *ACS Photonics* **3** 992
[25] Chen Y, Lee C, Lu L, Liu D, Wu Y K, Feng L T, Li M, Rockstuhl C, Guo G P, Guo G C, Tame M and Ren X F 2018 *Optica* **3** 992
[26] Slussarenko S, Weston M M, Chrzanowski H M, Shalm L K, Verma V B, Nam S W and Pryde G J2017 *Nat. Photonics* **11** 700
[27] Nagata T, Okamoto R, Jeremy L O, Sasaki K and Takeuchi S 2007 *Science* **316** 726
[28] Wu C, Liu Y W, Gu X W, Xue S C, Yu X X, Kong Y C, Qiang X G, Wu J J, Zhu Z H and Xu P 2019 *Chin. Phys. B* **28** 104211
[29] Hong C K, Ou Z Y and Mandel L 1987 *Phys. Rev. Lett.* **59** 2044
[30] Okamoto R, Hofmann H F, Nagata T, O'Brien J L, Sasaki K and Takeuchi S 2008 *New J. Phys.* **10** 73033